JOURNAL OF CHEMICAL INFORMATION AND MODELING

Article

pubs.acs.org/jcim

Integrative and Personalized QSAR Analysis in Cancer by Kernelized Bayesian Matrix Factorization

Muhammad Ammad-ud-din,*[,†] Elisabeth Georgii,[†] Mehmet Gönen,[†] Tuomo Laitinen,[‡] Olli Kallioniemi,[§] Krister Wennerberg,[§] Antti Poso,[‡,∥] and Samuel Kaski*[,†,⊥]

[†]Helsinki Institute for Information Technology HIIT, Department of Information and Computer Science, Aalto University, P.O. Box 15400, Espoo 00076, Finland

[‡]School of Pharmacy, Faculty of Health Sciences, University of Eastern Finland, P.O. Box 1627, Kuopio 70211, Finland

[§]Institute for Molecular Medicine Finland FIMM, University of Helsinki, P.O. Box 20, Helsinki 00014, Finland

[∥]Division of Molecular Oncology of Solid Tumors, Department of Internal Medicine 1, University Hospital Tuebingen, Otfried Mueller-Strasse 10, 72076 Tuebingen, Germany

[⊥]Helsinki Institute for Information Technology HIIT, Department of Computer Science, University of Helsinki, P.O. Box 68, Helsinki 00014, Finland

Supporting Information

ABSTRACT: With data from recent large-scale drug sensitivity measurement campaigns, it is now possible to build and test models predicting responses for more than one hundred anticancer drugs against several hundreds of human cancer cell lines. Traditional quantitative structure−activity relationship (QSAR) approaches focus on small molecules in searching for their structural properties predictive of the biological activity in a single cell line or a single tissue type. We extend this line of research in two directions: (1) an integrative QSAR approach predicting the responses to new drugs for a panel of multiple known cancer cell lines simultaneously and (2) a personalized QSAR approach predicting the responses to new drugs for new cancer cell lines. To solve the modeling task, we apply a novel kernelized Bayesian matrix factorization method. For maximum applicability and predictive performance, the method optionally utilizes genomic features of cell lines and target information on drugs in addition to chemical drug descriptors. In a case study with 116 anticancer drugs and 650 cell lines, we demonstrate the usefulness of the method in several relevant prediction scenarios, differing in the amount of available information, and analyze the importance of various types of drug features for the response prediction. Furthermore, after predicting the missing values of the data set, a complete global map of drug response is explored to assess treatment potential and treatment range of therapeutically interesting anticancer drugs.

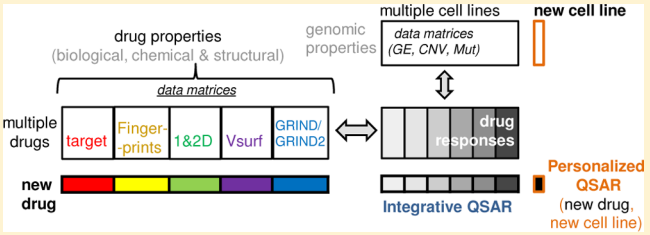

INTRODUCTION

Several recent large-scale high-throughput screening efforts provide drug sensitivity measurements for a whole panel of human cancer cell lines and dozens of drugs. So far, these data have been used in search for dependencies between genomic features and drug responses, addressing the personalized medicine task.

The core computational problem of personalized medicine is the following: given genomic features of the cell lines and their sensitivity measurements from an *a priori* fixed set of drugs, predict sensitivity of a new cell line to these drugs. In other words, the corresponding computational models are devised to generalize across cell lines (Figure 1A). In personalized medicine research, a variety of features have been studied for genomic characterization of cell lines. These features include gene expression, copy number variation, and mutational status of the cell lines. For model learning, several statistical methods have been applied, most commonly multivariate linear regression (using LASSO and elastic net regularizations) and nonlinear regression (e.g., neural networks and kernel methods).[1−5]

On the other hand, quantitative structure−activity relationship (QSAR) methods investigate structural properties of drug molecules regarding their effects on the drug's biological activity for an *a priori* fixed set of target cells.[6] The resulting computational models can be used for predicting the activity of drug compounds outside the data set, i.e., they have been designed to generalize across drugs (Figure 1B). Statistical methods for learning such models are described in the next paragraph. Our work focuses on QSAR analysis of cancer drugs and extends the traditional QSAR approach in two directions: (1) an integrative QSAR approach, where the responses to new drugs are predicted for a panel of representative cancer cell lines simultaneously, and (2) a personalized QSAR approach, where the responses to both new and established drugs are

Received: March 10, 2014

   dx.doi.org/10.1021/ci500152b | J. Chem. Inf. Model. XXXX, XXX, XXX−XXX

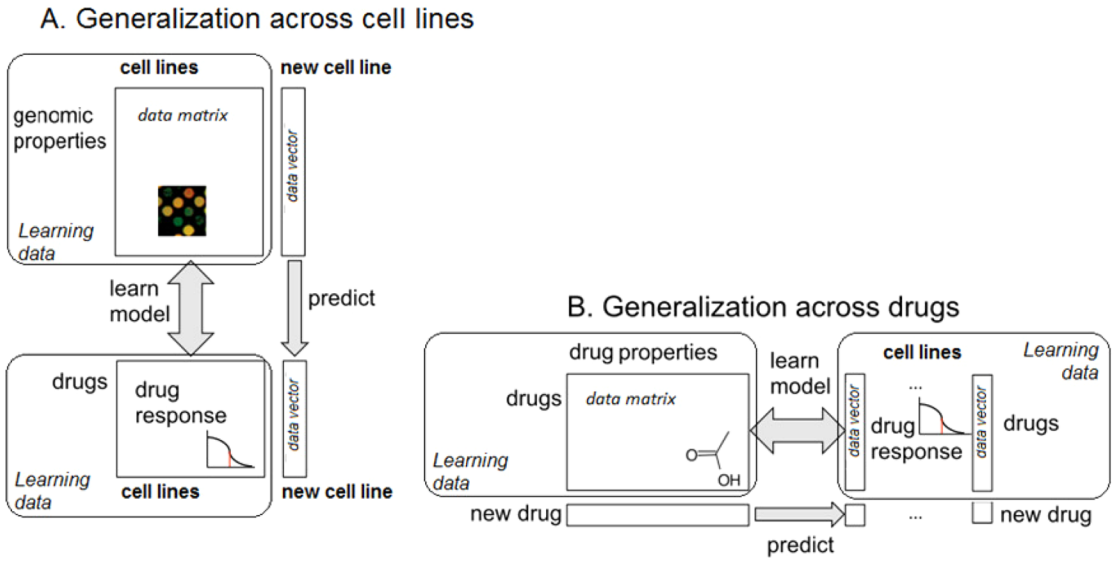

Figure 1. Two complementary approaches of exploiting high-throughput drug screening data from cancer cell lines. (A) Personalized medicine approach (generalization across cell lines): given genomic properties of a cell line, predict the cell line's responses to a fixed set of drugs. (B) QSAR approach (generalization across drugs): given chemical and structural properties of a drug, predict the response of this drug in a fixed set of cell lines. Each approach consists of two different steps. The first step is to learn a model that describes the relationship between drug responses and genomic (or chemical) properties. In the second step, the model is used to make predictions for new data with unknown response values. Methods to learn these models are described in the main text. This paper extends approach B (Figure 2).

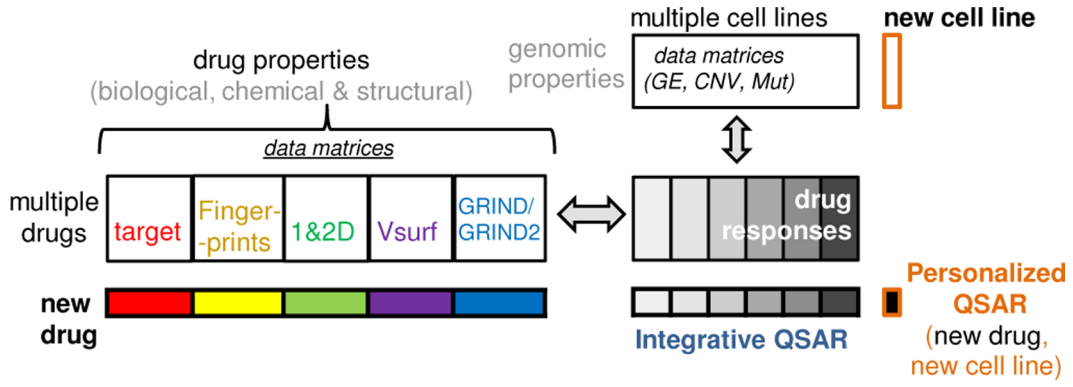

Figure 2. Extended QSAR analysis approach for cancer drug response prediction proposed in this work. Traditional QSAR analysis predicts efficacies of new cancer drugs from drug properties (Figure 1B). The proposed approach additionally integrates side information on the cell lines for which drug responses are predicted; here, the side information consists of genomic characteristics of the cell lines. With this approach, two new tasks can be performed: (1) integrative QSAR analysis: predicting drug efficacy for multiple cell lines simultaneously and (2) personalized QSAR analysis: predicting drug efficacy for a new cell line. In the figure, each block represents a data matrix. The matrix of drug response values has one row per drug and one column per cell line. The side information for drugs is given by a set of matrices, each of which represents the drugs as rows and drug features of a specific type as columns. Here, five drug feature types are considered: biological targets, fingerprints, 1D and 2D descriptors, Vsurf, and GRIND/GRIND2. The contents of these data matrices are binary or quantitative values characterizing a specific drug with respect to the specific features. The side information matrix for cell lines contains cell lines as columns and genomic features as rows (GE, gene expression; CNV, copy number variation; and Mut, cancer gene mutations). Only one block is shown to save space.

predicted for new cancer cell lines. The latter extension is developed with the motivation to eventually be applied to primary cancer cell lines. Both extensions are tested thoroughly using the data from the Sanger Genomics of Drug Sensitivity in Cancer project.[1,7]

Two lines of research are crucial in the QSAR field: (1) the development of suitable descriptors capturing chemical and physical properties of drug molecules and (2) the development of statistical methods to learn prediction models. The available descriptors range from 2D fingerprints to spatial features and physiochemical properties.[6,8,9] This paper contributes to the second line, development of statistical methods, aiming at models that relate the descriptors to biological activity. Previous work includes linear methods (e.g., multivariate linear regression, partial least-squares PLS, principal component regression PCR) as well as nonlinear methods (kernel methods, neural networks). In the specific problem of QSAR analysis for cancer drugs, multivariate linear regression, PLS, PCR, kernel methods, and neural network type methods have been widely applied. Linear approaches are most prominent in QSAR analysis.[6,8] Multivariate linear regression has been used in numerous studies[10−12] including analysis of antiproliferative activity of compounds in human cancer cells.[13] A major challenge in the analysis is that structural descriptors can be highly correlated, and the number of descriptors is large, often exceeding the number of chemical compounds available for

dx.doi.org/10.1021/ci500152b | J. Chem. Inf. Model. XXXX, XXX, XXX−XXX

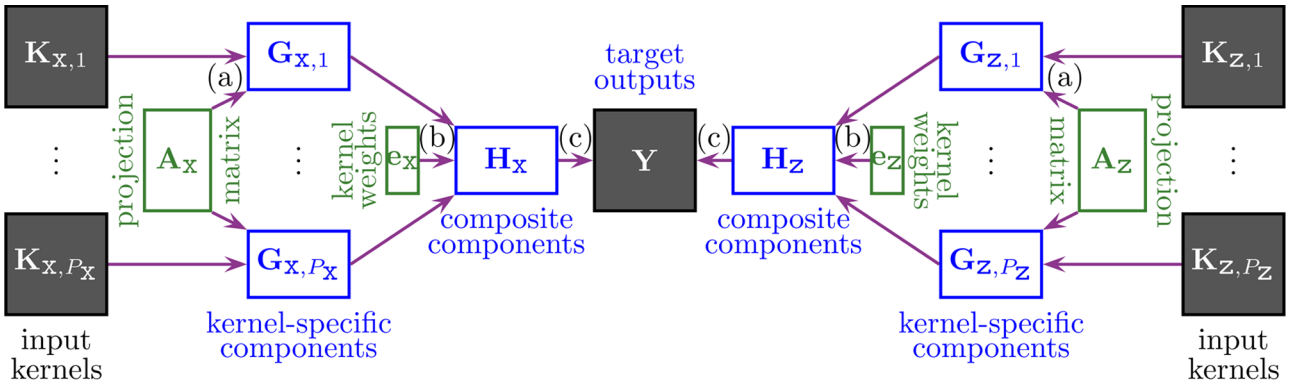

Figure 3. Flowchart of kernelized matrix factorization with multiple kernel learning. From each of the side information data types for drugs illustrated in Figure 2, a pairwise similarity matrix (kernel) between all the drugs in the training data set is computed ($K_{X,1}...K_{X,P_X}$; left border of image). The model produces a low-dimensional representation of drugs $G_{X,1}...G_{X,P_X}$, obtained from each kernel utilizing a common projection matrix A_X (kernel-based nonlinear dimensionality reduction, see text). A weighted combination of the matrices $G_{X,1}...G_{X,P_X}$ parametrized by the weight vector e_X (one weight coefficient per kernel) yields the composite component matrix H_X (multiple kernel learning, see text). In the same way, a composite component matrix H_Z is obtained from kernels between cell lines, depicted on the right half of the figure. The output matrix Y (here, containing drug responses) is calculated as a matrix product of H_X and H_Z (matrix factorization, see text). The gray shaded nodes are given by the training data. The green nodes are the parameters to be learned. The blue nodes are the latent representations used by the model. See main text for more details.

training. There exist several ways to deal with these problems. A frequent solution is to combine linear regression with feature selection techniques.[14−16] In addition, sparsity of linear regression models can be enforced by employing LASSO or elastic net regularization.[11] Another common strategy is principal component regression (PCR),[6] which consists of a two-step procedure. In the first step, the top principal components of the descriptor data are computed to obtain a low-dimensional data representation by linear combinations of the original descriptors. This representation is used in the second step as input to the regression model. The main idea of partial least-squares (PLS) is similar to that of PCR. However, PLS additionally exploits the output values to construct the linear combinations of the descriptors. PLS has been introduced to the QSAR field with comparative molecular field analysis (CoMFA)[17] and has been highly popular ever since.[8,18] Also PLS methods for multivariate output values have been used for QSAR studies.[18] In cancer analysis, PLS has been applied to connect compound activity to genomic properties of cells.[19] Beyond the linear methods, nonlinear QSAR analysis has been studied. One approach is kernel regression. For example, Yamanishi et al.[20] predicted drug side effects from the chemical structure and the target information on drugs using multiple kernel regression. An alternative approach for nonlinear QSAR analysis are neural networks.[21] Sutherland et al.[22] compared a neural network-based QSAR model with other commonly known QSAR methods using benchmark data sets. Their study reported that neural networks are equally or more predictive than PLS models when used with a basic set of 1D and 2D descriptors. However, with the availability of high-dimensional data, the feasibility of simpler models such as traditional neural networks depends on appropriate preselection of features to reduce the dimensionality of the data. Recently, deep learning methods utilizing high-dimensional data have been studied for general QSAR problems in chemoinformatics. Lusci et al.[23] demonstrated a recursive approach for modeling deep architectures for the prediction of molecular properties and illustrate the usefulness of their approach on the problem of predicting aqueous solubility. The method proposed in this paper is also applicable to the general QSAR problem in chemoinformatics and is fully equipped to deal with high dimensionality of the data.

We present a novel matrix factorization method to address the task of QSAR analysis in cancer. The method goes beyond the existing work in this application field in two main aspects (Figure 2). First, multiple cancer cell lines are integrated into one model, instead of building separate models for individual cell types[13,24] or averaging across the cancer cell lines.[25] This results in an integrative QSAR prediction, i.e., the columns of the drug response matrix in Figure 2 are predicted together (not one by one independently), making it possible to utilize their commonalities. Second, the model utilizes biological information not only in the form of known targets as additional drug features but also in the form of genomic profiles of the cell lines. This allows us to also make predictions for untested drugs on new cell lines (i.e., cell lines outside the training set). This can be viewed as personalized QSAR prediction, which has not been addressed earlier and is a new research problem (Figure 2).

Technically, the method we propose for this task can be regarded as a type of generalized "recommender system", incorporating both side information on drugs (corresponding to items) and side information on cell lines (corresponding to users). In previous work, matrix factorization-based collaborative filtering, a popular approach in product recommendation that does not use any side information, proved useful for predicting missing values of compound activity in multiple cell lines.[26] Generalizing the matrix factorization to include side information on both sides allows maximum flexibility in the various prediction scenarios. In recommender system terminology, the integrative QSAR prediction corresponds to making recommendations for the use of untested *cold-start* compounds across the different cancer types, whereas the personalized QSAR prediction considers cold-start compounds in combination with a cold-start cell line. Our recommender system is based on the kernelized Bayesian matrix factorization method (KBMF), which was originally introduced for drug−protein interaction analysis[27] and has been extended to use multiple

dx.doi.org/10.1021/ci500152b | J. Chem. Inf. Model. XXXX, XXX, XXX−XXX

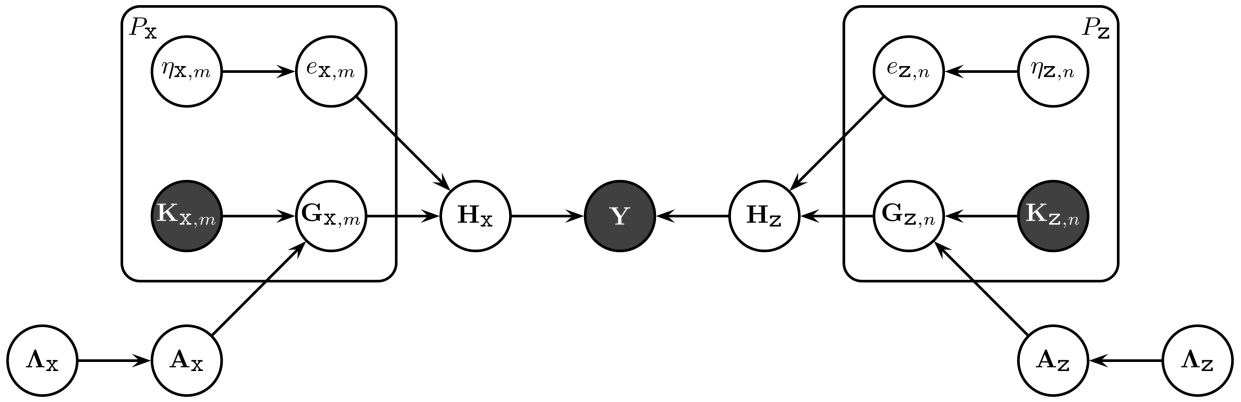

Figure 4. Graphical model of kernelized Bayesian matrix factorization (KBMF) with multiple kernel learning. The figure demonstrates the latent variables with their priors. In particular, $\Lambda_{(.)}$ denotes the matrices of priors for the entries of the projection matrices $A_{(.)}$. $\eta_{(.,.)}$ represents vectors of priors for the kernel weights $e_{(.,.)}$. See text for more details on distributional assumptions.

types of side information.[28] We present a case study on drug response data from the Wellcome Trust Sanger Institute.[7] As side information for drugs, we use 1D, 2D, and 3D descriptors as well as protein targets. The side information for cell lines includes gene expression, copy number variation, and mutation data. The method learns an importance weight for each data type and is implemented as a Bayesian model, solving the extended QSAR problem by probabilistic modeling. The kernel-based formulation allows for nonlinear relationships in the QSAR analysis.

MATERIALS AND METHODS

Kernelized Bayesian Matrix Factorization (KBMF). Drugs and cell lines are assumed to come from two domains $\mathcal{X}$ and $\mathcal{Z}$, respectively. We assume two samples of independent and identically distributed training instances from each domain, denoted by $X = \{\vec{x}_i \in \mathcal{X}\}_{i=1}^{N_x}$ and $Z = \{\vec{z}_j \in \mathcal{Z}\}_{j=1}^{N_z}$. For calculating similarities, we use multiple kernel functions for each domain, namely, $\{k_{x,m}: \mathcal{X} \times \mathcal{X} \to \mathbb{R}\}_{m=1}^{P_x}$ and $\{k_{z,n}: \mathcal{Z} \times \mathcal{Z} \to \mathbb{R}\}_{n=1}^{P_z}$. The set of kernels may correspond to different notions of similarity on the same feature representation or may use information coming from multiple feature representations (i.e., views). The (i,j)th entry of the output matrix $Y \in \mathbb{R}^{N_x \times N_z}$ gives the drug response measurement between drug x_i and cell line z_j.

Figure 3 illustrates the method we use; it is composed of three main parts included in one unified model: (a) kernel-based nonlinear dimensionality reduction, (b) multiple kernel learning, and (c) matrix factorization. First, we briefly explain each part and introduce the notation. We then formulate a probabilistic model and derive a variational approximation for learning and predictions.

Kernel-Based Nonlinear Dimensionality Reduction. This part performs feature extraction using the input kernel matrices $\{K_{x,m} \in \mathbb{R}^{N_x \times N_x}\}_{m=1}^{Px}$ and a common projection matrix $A_x \in \mathbb{R}^{N_x \times R}$, where R is the resulting subspace dimensionality. The projection gives kernel-specific components $\{G_{x,m} = A_x^{\top} K_{x,m}\}_{m=1}^{Px}$. The main idea is very similar to *kernel principal component analysis* or *kernel Fisher discriminant analysis*, where the columns of the projection matrix can be solved with eigen decompositions.[29] However, this solution strategy is not possible for the more complex model formulated here.

Having a shared projection matrix across the kernels has two main implications: (i) The number of model parameters is much lower than if we had a separate projection matrix for each kernel, leading to more regularization. (ii) We can combine the kernels with multiple kernel learning as explained in the following.

Multiple Kernel Learning. This part is responsible for combining the kernel-specific (i.e., view-specific) components linearly to obtain the *composite components* $H_x = \sum_{m=1}^{Px} e_{x,m} G_{x,m}$, where the kernel weights can take arbitrary values $e_x \in \mathbb{R}^{P_x}$. The multiple kernel learning property of this formulation can easily be seen from the following equivalence

$$\sum_{m=1}^{P_x} e_{x,m} \underbrace{(A_x^{\top} K_{x,m})}_{G_{x,m}} = A_x^{\top} \underbrace{\left(\sum_{m=1}^{P_x} e_{x,m} K_{x,m} \right)}_{\text{combined kernel}}$$

where we need to have a shared projection matrix to obtain a valid linear combination of the kernels.

Matrix Factorization. In this part, the low-dimensional representations of objects in the unified subspace, namely, H_x and H_z, are used to calculate the output matrix $Y = H_x^{\top} H_z$. This corresponds to factorizing the outputs into two low-rank matrices.

Kernelized Bayesian matrix factorization (KBMF) is a probabilistic model formulated to solve this prediction task. It has two key properties that enable us to perform efficient inference: (i) The kernel-specific and composite components are modeled explicitly by introducing them as latent variables. (ii) Kernel weights are assumed to be normally distributed without enforcing any constraints (e.g., non-negativity) on them.

Figure 4 shows the graphical model of KBMF with the latent variables and their priors. There are some additions to the notation described earlier: The $N_x \times R$ and $N_z \times R$ matrices of priors for the entries of the projection matrices A_x and A_z are denoted by Λ_x and Λ_z, respectively. The $P_x \times 1$ and $P_z \times 1$ vectors of priors for the kernel weights e_x and e_z are denoted by η_x and η_z, respectively. The standard deviations for the kernel-specific components, composite components, and target outputs are σ_g, σ_h, and σ_y, respectively; these hyperparameters are not shown for clarity.

Next, we specify the distributional assumptions of the model. The central assumptions are normal distribution of the noise

dx.doi.org/10.1021/ci500152b | J. Chem. Inf. Model. XXXX, XXX, XXX−XXX

and the dependencies shown in Figure 4; the other assumptions are technical details made for analytical and computational convenience and can be replaced if needed. As the goal is to predict, these assumptions ultimately become validated by prediction performances on the test data (Results section). In the equations, matrices are denoted by capital letters, with the subscript x or z indicating the data domain (drugs or cells, respectively); matrix entries are denoted by noncapital letters, with the row index as superscript and the column index as the last subscript (i.e., $a^i_{x,s}$ denotes the entry at (row i, column s) of matrix A_x).

The distributional assumptions of the dimensionality reduction part are

$$\lambda^i_{x,s} \sim \mathcal{G}(\lambda^i_{x,s};\alpha_\lambda,\beta_\lambda) \quad \forall\ (i,\ s)$$

$$a^i_{x,s}|\lambda^i_{x,s} \sim \mathcal{N}(a^i_{x,s};0,(\lambda^i_{x,s})^{-1}) \quad \forall\ (i,s)$$

$$g^s_{x,m,i}|a_{x,s},k_{x,m,i} \sim \mathcal{N}(g^s_{x,m,i};a^{\mathrm{T}}_{x,s}k_{x,m,i},\sigma^2_g) \quad \forall\ (m,s,i)$$

where $\mathcal{N}(\cdot;\mu,\Sigma)$ is the normal distribution with mean vector μ (here scalar) and covariance matrix $\sum$ (here scalar), and $\mathcal{G}(\cdot{:}\alpha,\beta)$ denotes the gamma distribution with shape parameter α and scale parameter β. The multiple kernel learning part has the following distributional assumptions

$$\eta_{x,m} \sim \mathcal{G}(\eta_{x,m};\alpha_\eta,\beta_\eta) \quad \forall\ m$$

$$e_{x,m}|\eta_{x,m} \sim \mathcal{N}(e_{x,m};0,\eta^{-1}_{x,m}) \quad \forall\ m$$

$$h^s_{x,i}|\{e_{x,m},g^s_{x,m,i}\}_{m=1}^{P_x} \sim \mathcal{N}(h^s_{x,i};\sum_{m=1}^{P_x} e_{x,m}g^s_{x,m,i},\sigma^2_h) \quad \forall\ (s,\ i)$$

where kernel-level sparsity can be tuned by changing the hyperparameters (α_η,β_η). Setting the gamma priors to induce sparsity, e.g., $(\alpha_\eta,\ \beta_\eta)$ = (0.001, 1000), produces results analogous to using the l_1-norm on the kernel weights, whereas using uninformative priors, e.g., $(\alpha_\eta,\ \beta_\eta)$ = (1, 1), resembles using the l_2-norm. The matrix factorization part calculates the target outputs using the inner products between the low-dimensional representations of the object pairs:

$$y^i_j|h_{x,i},h_{z,j} \sim \mathcal{N}(y^i_j;h^{\mathrm{T}}_{x,i}h_{z,j},\sigma^2_y) \quad \forall\ (i,j) \in \mathcal{I}$$

where I is the index set that contains the indices of observed entries in Y.

Exact inference for the model is intractable, and among the two readily available approximative alternatives, Gibbs sampling and variational approximation, we choose the latter for computational efficiency.[28] Variational methods optimize a lower bound on the marginal likelihood, which involves a factorized approximation of the posterior, to find the joint parameter distribution.[30]

The source code of the method is available as a Matlab package at http://research.ics.aalto.fi/mi/software/kbmf/.

Benchmark QSAR Data Sets. A total of eight standard QSAR data sets were used in the benchmark study.[22] The data sets include (1) angiotensin converting enzyme inhibitors (ACE data set), (2) acetylcholinesterase inhibitors (AchE), (3) benzodiazepine receptor ligands (BZR), (4) cyclooxygenase-2 inhibitors (COX2), (5) dihydrofolate reductase inhibitors (DHFR), (6) inhibitors of glycogen phosphorylase b (GPB), (7) thermolysin inhibitors (THER), and (8) thrombin inhibitors (THR). The details on these data sets including the number of compounds and the utilized 2.5D descriptors are presented in Table-S1 under the given acronyms (Supporting Information). The data sets were downloaded from the Supporting Information provided by Sutherland et al.[22]

Drug Response Data. We used the data from the Genomics of Drug Sensitivity in Cancer project[1,7] by Wellcome Trust Sanger Institute (version release 2.0, July 2012) consisting of 138 drugs and a panel of 790 cancer cell lines. Drug sensitivity measurements were summarized by log-transformed IC_{50} values (the drug concentration yielding 50% response, given as natural log of μM). In addition, cell lines were characterized by a set of genomic features. We selected the 650 cell lines for which both drug response data and complete genomic characterization were available. Furthermore, we focused on the 116 drugs for which SDF or MDL format (encoding the chemical structure of the drugs) were available from the NCBI PubChem Repository[31] to be able to compute chemical drug descriptors. The resulting drug response matrix of 116 drugs by 650 cell lines has 75,400 entries, out of which 19,781 (26%) are missing. The used data and value range were chosen to be consistent with earlier publications.[1,4]

Drug Features. As the KBMF model can incorporate multiple types of side information, we computed several types of chemical descriptors for the drugs. First, we computed PubChem fingerprint descriptors using the PaDEL software[32,33](v2.17, downloaded from the project Web site), capturing occurrence of fragments in the 2D structure. In addition, we calculated the 1D and 2D descriptors available in PaDEL software using default settings. The 1D descriptors are summaries of compositional or constitutional molecular properties, e.g., atom count, bond count, and molecular weight. The 2D descriptors encode different quantitative properties of the topology.[32,33] Lastly, we considered two types of 3D descriptors focusing on spatial and physiochemical properties of the drugs, namely, Vsurf and GRIND/GRIND2. The 2D structures were converted into 3D structures using the LigPrep module of the Schrödinger Maestro software package (Version 2.5, Schrödinger, LLC, New York, 2012). A few inorganic substances were not successfully converted due to missing molecular parameters. A full set of Vsurf descriptors was calculated from the 3D molecular database using Molecular Operating Environment software (MOE, Version 2012.10).[34] Vsurf descriptors are generally used to describe the molecular size and shape of hydrophilic and hydrophobic regions. The Pentacle software (version 1.0.6. Molecular Discovery, Ltd., Middlesex, U.K.) was applied to calculate GRIND and GRIND2 descriptors.[35−37] First, 3D maps of interaction energies between the molecule and chemical probes were calculated. Second, these 3D interaction maps were further converted into GRIND and GRIND2 descriptors, which do not require alignment of compounds. In a preprocessing step, we removed all features with constant values across all drugs, obtaining the final set of features for each type listed in Table S-3 of the Supporting Information. In addition to these chemical and structural descriptors, we obtained drug target information from the Genomics of Drug Sensitivity in Cancer project[7] and encoded it as a binary drug versus target matrix. In addition to individual target proteins, target families and effector pathways were included. For each type of drug features, a kernel matrix was computed, containing pairwise similarities of drugs with respect to the specific feature type. For the binary features

dx.doi.org/10.1021/ci500152b | J. Chem. Inf. Model. XXXX, XXX, XXX−XXX

Table 1. KBMF Test Set Performance Comparison against State-of-the-Art QSAR Methods Using Benchmark QSAR Data Sets[a]

data set		KBMF	PLS	GFA-l	GFA-l-ens	GFA-nl	GFA-nl-ens	GPLS	GPLS-ens	NN	NN-ens
ACE	R^2_{test}	**0.57**	0.51	0.49	0.50	0.39	0.32	0.45	0.43	0.39	0.51
	s_{test}	**1.40**	1.50	1.53	1.51	1.68	1.77	1.60	1.62	1.68	1.51
	MSE ± SEM (std)	**1.12 ± 0.42 (1.58)**	2.22	2.31	2.25	2.80	3.11	2.53	2.60	2.80	2.25
AchE	R^2_{test}	0.31	0.16	0.16	0.22	0.29	**0.40**	0.13	0.14	−0.04	0.21
	s_{test}	1.10	1.20	1.20	1.15	1.10	**1.01**	1.22	1.21	1.34	1.16
	MSE ± SEM (std)	1.16 ± 0.26 (1.63)	1.41	1.41	1.30	1.18	**0.99**	1.46	1.44	1.77	1.32
BZR	R^2_{test}	0.22	0.20	0.22	0.21	0.20	0.20	0.20	0.18	**0.39**	0.34
	s_{test}	0.86	0.87	0.86	0.86	0.87	0.87	0.87	0.88	**0.76**	0.79
	MSE ± SEM (std)	0.68 ± 0.17 (1.18)	0.74	0.72	0.72	0.74	0.74	0.74	0.75	**0.56**	0.60
COX2	R^2_{test}	**0.33**	0.27	0.28	0.25	0.12	0.13	0.28	0.26	0.31	0.32
	s_{test}	**1.20**	1.25	1.24	1.27	1.37	1.37	1.24	1.26	1.22	1.21
	MSE ± SEM (std)	**1.13 ± 0.24 (2.34)**	1.55	1.53	1.60	1.87	1.87	1.53	1.58	1.48	1.45
DHFR	R^2_{test}	**0.57**	0.49	0.46	0.48	0.50	0.53	0.49	0.53	0.42	0.54
	s_{test}	**0.91**	0.99	1.01	1.00	0.98	0.95	0.99	0.94	1.05	0.94
	MSE ± SEM (std)	**0.84 ± 0.11 (1.19)**	0.97	1.01	0.99	0.95	0.89	0.97	0.88	1.09	0.88
GPB	R^2_{test}	**0.42**	0.04	−0.02	0.15	−0.08	0.14	0.04	0.01	0.28	0.25
	s_{test}	**0.94**	1.20	1.25	1.14	1.28	1.14	1.21	1.23	1.05	1.07
	MSE ± SEM (std)	**0.86 ± 0.26 (1.22)**	1.39	1.52	1.25	1.59	1.25	1.42	1.47	1.06	1.10
THER	R^2_{test}	0.07	0.07	0.20	0.30	0.16	0.21	0.33	**0.33**	0.16	0.19
	s_{test}	2.20	2.24	2.08	1.95	2.13	2.07	1.91	**1.90**	2.13	2.10
	MSE ± SEM (std)	4.97 ± 0.45 (2.24)	4.98	4.29	3.76	4.50	4.24	3.61	**3.57**	4.50	4.37
THR	R^2_{test}	**0.36**	0.28	0.13	0.27	0.11	0.12	0.11	0.16	0.26	0.23
	s_{test}	**0.91**	0.96	1.06	0.97	1.07	1.07	1.08	1.04	0.98	1.00
	MSE ± SEM (std)	**0.80 ± 0.24 (1.27)**	0.89	1.09	0.91	1.11	1.11	1.13	1.05	0.93	0.97

[a]Performance indicators of partial least squares (PLS), genetics function approximation (GFA), GFA with linear terms (GFA-l), GFA ensemble models with linear terms (GFA-l-ens), GFA with nonlinear terms (GFA-nl), GFA ensemble models with nonlinear terms (GFA-nl-ens), PLS models with descriptor selection via GFA (GPLS), ensemble of PLS models with descriptor selection via GFA (GPLS-ens), neural networks (NN), and ensemble of neural network models (NN-ens) were taken from the work by Sutherland et al.[22] using their Table 5. The KBMF method used the same training and test sets as the others. The best result for each data set is marked in bold. Additionally, we provide the pooled mean squared error with standard error of the mean (SEM) and standard deviation (in brackets). For the comparison methods, detailed statistics are not available, and we computed only MSE from the s_{test} value.

(targets and fingerprints), the Jaccard coefficient was used; for all other feature types, a Gaussian kernel was computed.

Cell Line Features. Three types of genomic profiles were included in the Genomics of Drug Sensitivity in Cancer project[1] to characterize the cell lines: gene expression, copy number and mutation profiles. Gene expression profiles quantize the transcript levels of genes, whereas copy number profiles measure the amplification or deletion of genes in the DNA and mutation profiles state changes in the sequence of a gene. While the gene expression and copy number profiles are genome-wide, the mutation data focus on cancer gene mutations and relate to somatic mutations frequently occurring in tumors. In the Genomics of Drug Sensitivity in Cancer project,[1] the gene expression measurements were made using HT-HGU122A Affymetrix whole genome array, copy number variants were obtained through SNP6.0 microarrays, and cancer gene mutations were determined using the capillary sequencing technique. We included all three data types in our analysis, using the same data as the elastic net analysis in the pilot study, accessible from Genomics of Drug Sensitivity in Cancer project's Web site.[7] Analogous to the preprocessing of drug features, we removed the features with constant values across all cell lines. The number of features for each type is given in Table S-4 of the Supporting Information. To obtain a kernel representation, the Jaccard similarity coefficient was used for mutation data and Gaussian kernels for gene expression and copy number data.

RESULTS AND DISCUSSION

Performance Evaluation on Benchmark QSAR Data sets. We started by verifying that in the standard QSAR task, where the new approaches do not have a competitive advantage, the performance of the new KBMF method was comparable to state-of-the-art QSAR methods. We evaluated the methods using the eight benchmark data sets with training data, test data, and descriptors provided by Sutherland et al.[22] in their comparison study. During training, a nested cross-validation experiment was performed to select the optimal number of components for KBMF, which was subsequently used for predictions on the test set. Details can be found in the text and Table S-2 of the Supporting Information. Table 1 lists the performance on the test sets, using the same evaluation criteria as reported in the earlier benchmark experiment,[22] coefficient of determination (R^2_{test}), and standard error of predictions (s_{test}). Additionally, we provide error statistics for KBMF. Regarding the summary performance measures, the KBMF method achieves the best results among all methods in five out of eight data sets, showing that KBMF performance matches the state-of-the-art. Like the other methods, KBMF achieves the best prediction performance for the data sets ACE and DFHR, and in both cases, it has better performance values than the other methods. For the BZR data set, KBMF and GFA-l have comparable performance, following NN and NN-ens. Sutherland et al.[22] reported the presence of outlier compounds in this data set. Removing outliers as described there, the R^2_{test} and s_{test} improved to 0.49 and 0.67, respectively,

dx.doi.org/10.1021/ci500152b | J. Chem. Inf. Model. XXXX, XXX, XXX−XXX

outperforming NN and NN-ens. In the THER data set, the performance of KBMF is comparable to PLS but lower than for the remaining methods. One potential reason for the better performance of the other methods on this specific data set is that they preselect relevant features. Feature selection is necessary for the feasibility of GFA and traditional NN type of models, whereas deep and recursive NN, PLS, and KBMF can operate on the full data with high dimensionality. It is plausible that performance of KBMF could also improve with suitable feature selection, but this investigation is left to future work.

Integrative QSAR Prediction of Drug Responses across Multiple Cancer Cell lines. We next present an integrative QSAR analysis on the drug response data from the Genomics of Drug Sensitivity in Cancer (GDSC) project.[7] Unlike the benchmark QSAR applications, which have a single output variable, the drug sensitivity study investigates the efficacy of compounds across a set of different cell lines and cancer types. Rather than looking at each cell line one by one, a natural extension of QSAR analysis considers all cell lines simultaneously in one unified model, which is implemented by the KBMF method. We utilized 1D, 2D, and 3D drug descriptors for predicting the response of left-out drugs (8-fold cross validation). The number of components in the KBMF method was fixed to 45 for all experiments on the GDSC data, which corresponds to a dimensionality reduction of about 60 percent relative to the smaller dimension of the response matrix (here, the number of drugs). Three different evaluation measures are reported on the test data: (1) mean squared error (MSE), (2) coefficient of determination R^2, and (3) Pearson correlation R_p. We complement the MSE value with estimates of standard errors and standard deviations. The cross-validation statistics for these evaluation measures can be found in Table S-5 of the Supporting Information.

Improved Performance by Incorporating Biological Information. In addition to the 1D, 2D, and 3D chemical and structural descriptors of drugs, we incorporated biological features into the model in the form of (1) target information for the drugs and (2) genomic properties of cell lines, both provided by the Genomics of Drug Sensitivity in Cancer project.[7] Neither of the two types of biological feature information is used in traditional QSAR approaches. We note that integrating the target information is easy in all QSAR approaches. However, simultaneous integration of genomic information has not been reported with any state-of-the-art QSAR methods for this prediction task. Our analysis shows that providing biological information to the model increases the prediction performance (see Table 2 and Table S-5 of the Supporting Information for cross-validation statistics). The predictive performance of the method $KBMF_{DD+TR+CF}$ is significantly higher than the other methods with a p-value <0.01 (Tables S6 and S7, Supporting Information). In terms of absolute performance, R^2 and R_p are at moderate levels but significantly better than baseline methods that take the mean of the training data as the prediction for a new drug (baseline1: cell line-specific mean; baseline2: overall mean). Therefore, we can conclude that KBMF is appropriate to address the novel and challenging task of predicting responses to new drugs for a panel of cell lines.

Relative Importance of Individual Drug Descriptor Types for Predicting Drug Responses. We investigated the contribution of each drug feature type to the task of predicting responses for test drugs left out from the training data. KBMF learns relevance weights $e_{x,m}$ for the different feature types. Figure 5 shows the average relevance weights across the eight models from cross-validation. The target information obtained the largest weight and the GRIND/GRIND2 descriptors the lowest weight. Remarkably, the relative ranking of feature types is conserved in all eight models (Figure S-1, Supporting Information), indicating the robustness of this relevance ordering. To analyze whether already a subset of feature types gives sufficient predictive power, we tested the performance of different combinations, adding feature types in the order of their learned weights (Table 3). While target information alone already achieves a considerable fraction of the overall performance, further performance gains are achieved by adding the other feature types, with the best result being obtained by the combination of all feature types (see Table 3 and Table S-8 of the Supporting Information for cross-validation statistics). Even though the differences in performances are quite small, the predictive performance obtained by the combination of all feature types is found to be significantly higher than the others with a p-value <0.01 (Tables S-9 and S-10, Supporting Information).

Table 2. Predicting Responses to New Drugs for a Panel of Known Cell Lines, Applying KBMF with Different Feature Sets[a]

method	MSE ± SEM (std)	R^2	R_p
$KBMF_{DD}$	0.83 ± 0.0053 (1.24)	0.21	0.47
$KBMF_{DD+TR}$	0.72 ± 0.0045 (1.07)	0.31	0.56
$KBMF_{DD+CF}$	0.80 ± 0.0051 (1.21)	0.23	0.49
$KBMF_{DD+TR+CF}$	**0.69 ± 0.0043 (1.01)**	**0.32**	**0.57**
baseline1 (cell linewise mean prediction)	1.03 ± 0.0061 (1.50)	0.00	0.03
baseline2 (overall mean prediction)	1.04 ± 0.0064 (1.52)	0.00	0.10

[a]MSE values with standard error of the mean (SEM) and standard deviations (in brackets) are shown. The subscript denotes the combination of feature types used in each of the experiments: DD = drug descriptors, TR = targets, and CF = cell features. The best result for each performance measure is marked in bold. The results indicate that biological features improve drug response prediction. Biological features can be either target information or genomic measurement data (neither are used in traditional QSAR analysis, but the former is easy to integrate into existing QSAR approaches).

Global Map of Drug Responses in Cancer. We will next discuss the global map of drug response in cancer produced by predicting missing values from the data. In the observed data, 26% of the measurements are missing, and we used KBMF to predict these missing values. We will begin by validating the performance of the method on missing value prediction, and then for more detailed analysis, we pick a set of therapeutically interesting drugs with reliable predictions. Therapeutic interestingness of the drugs is judged based on the selectivity of responses, and reliability was estimated by cross-validation on the existing measurements.

Performance on Missing Value Prediction. Up to now in this paper, we have investigated performances in predicting responses to previously unseen drugs. In practice, also the following prediction task is relevant: given response measurements for a drug in a subset of cell lines, predict drug responses on the remaining cell lines. In the context of recommender systems, this is called a *warm-start* prediction task because it can use partially known response values. We tested two warm-start prediction scenarios. In the blockwise approach, the same set of

dx.doi.org/10.1021/ci500152b | J. Chem. Inf. Model. XXXX, XXX, XXX−XXX

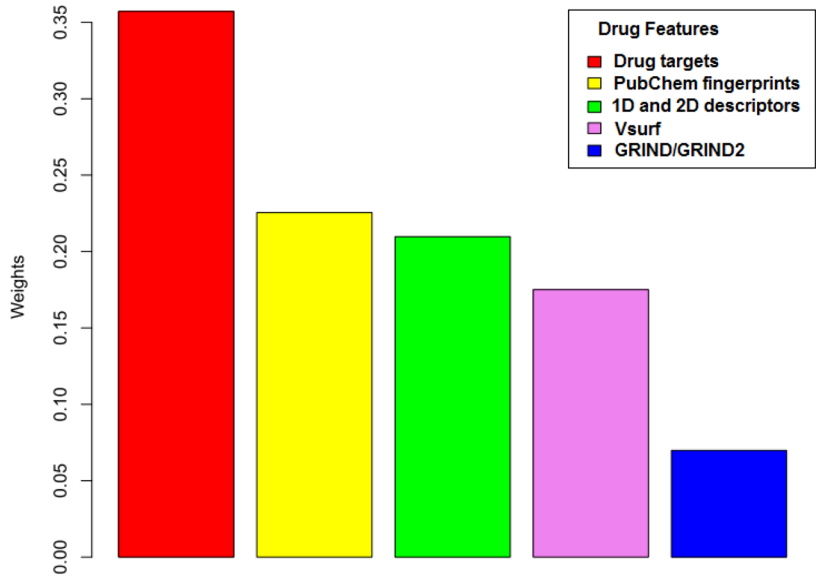

Figure 5. Relevance weights learned by the KBMF method for the different drug feature types averaged across the eight models from the cross-validation experiment. The ranking of feature types is conserved in the individual models (Figure S-1, Supporting Information).

Table 3. Prediction Results with Different Combinations of Feature Types[a]

feature type	MSE ± SEM (std)	R^2	R_p
targets	0.71 ± 0.0048 (1.13)	0.30	0.55
targets and fingerprints	0.73 ± 0.0045 (1.07)	0.30	0.56
targets, fingerprints, and 1D and 2D	0.72 ± 0.0045 (1.06)	0.31	0.56
targets, fingerprints, 1D and 2D and Vsurf	0.72 ± 0.0045 (1.06)	0.31	0.56
targets, fingerprints, 1D and 2D, Vsurf, and GRIND/GRIND2	**0.69 ± 0.0043 (1.01)**	**0.32**	**0.57**

[a]MSE values with standard error of the mean (SEM) and standard deviations (in brackets) are shown. Integration of all drug feature types gives the best result.

cell lines is missing for all drugs in the set of test drugs, whereas in the entrywise approach scattered drug-cell line combinations are predicted (Table 4 and Table S-11 of the Supporting Information). In both cases, the prediction performance is much better than when response values to the test drug are unknown for all cell lines (Table 2). That is, the method is able to exploit the additional available information to improve predictions. For our further analysis in the next section, we consider drugs based on the reliability of their predictions, as measured by MSE, focusing on the drugs with lower than average MSE in the entrywise prediction benchmark experiment.

Table 4. Performance on Missing Entry Prediction (a Warm-Start Prediction Task) Using the KBMF Method[a]

method	MSE ± SEM (std)	R^2	R_p
$KBMF_{blockwise}$	0.26 ± 0.0020 (0.47)	0.74	0.86
$KBMF_{entrywise}$	0.21 ± 0.0016 (0.37)	0.78	0.89

[a]Two different variants of the task are evaluated: predicting entries of a missing block (blockwise) and predicting scattered entries (entrywise). MSE values with standard error of the mean (SEM) and standard deviations (in brackets) are shown. Comparing to Table 2, note the additional performance gains when including known sensitivity measurements of the test drug on some cell lines into the model (and predicting for the remaining cell lines).

Insights from Novel Predictions. Using the method validated in the previous subsection, we trained a model on all available data and used it to predict the missing responses in the Sanger data set. We will next discuss insights from these predictions for the subset of drugs whose predictions are reliable (chosen as discussed in the previous subsection), exhibit tissue-selectivity of response (as evaluated by ANOVA), and are new findings (based on newly predicted values instead of existing data). In practice, we selected drugs with at least 20 newly predicted values, grouped cell lines based on their tissue origin, and measured selectivity of response by a one-way ANOVA test for each drug against these groups, retained drugs with p-value <0.05, and analyzed their tissue-specific effects. Effects are calculated as the difference between group mean and grand mean (*effect* = *group mean* − *grand mean*). Smaller values correspond to sensitive tissue types, and larger values correspond to resistant tissue types.

Figure 6 summarizes the tissue-specific effects of the selected drugs. In the figure, the drugs have been categorized into three groups of response patterns. Group 1 consists of drugs that are more effective on blood cancer than on lung cancer. This pattern is exhibited by nutlin-3a, palbociclib, nilotinib, SB590885, olaparib, veliparib, and bosutinib. According to the database at National Cancer Institute (NCI),[38] bosutinib has been approved for a certain type of blood cancer. Group 2 shows the reverse pattern of group 1, being more effective in lung than in blood cancer, and includes the drugs BI-D1870, ZM-447439, vorinostat, PD-173074, and BX-795. Group 3 contains drugs that are effective in more than one cancer types, namely, lapatinib, saracatinib, BMS-509744, WZ-1-84, and crizotinib. Lapatinib is approved for breast cancers but additionally seems to have a strong response in upper aerodigestive cancers. As another example, crizotinib is approved for lung cancers but appears to have some selective activities in CNS, upper aerodigestive, and GI tract cancers. Figures S-2 and S-3 of the Supporting Information show the heatmaps of the predicted response values for these selected drugs across cell lines from the seven major tissue types.

dx.doi.org/10.1021/ci500152b | J. Chem. Inf. Model. XXXX, XXX, XXX−XXX

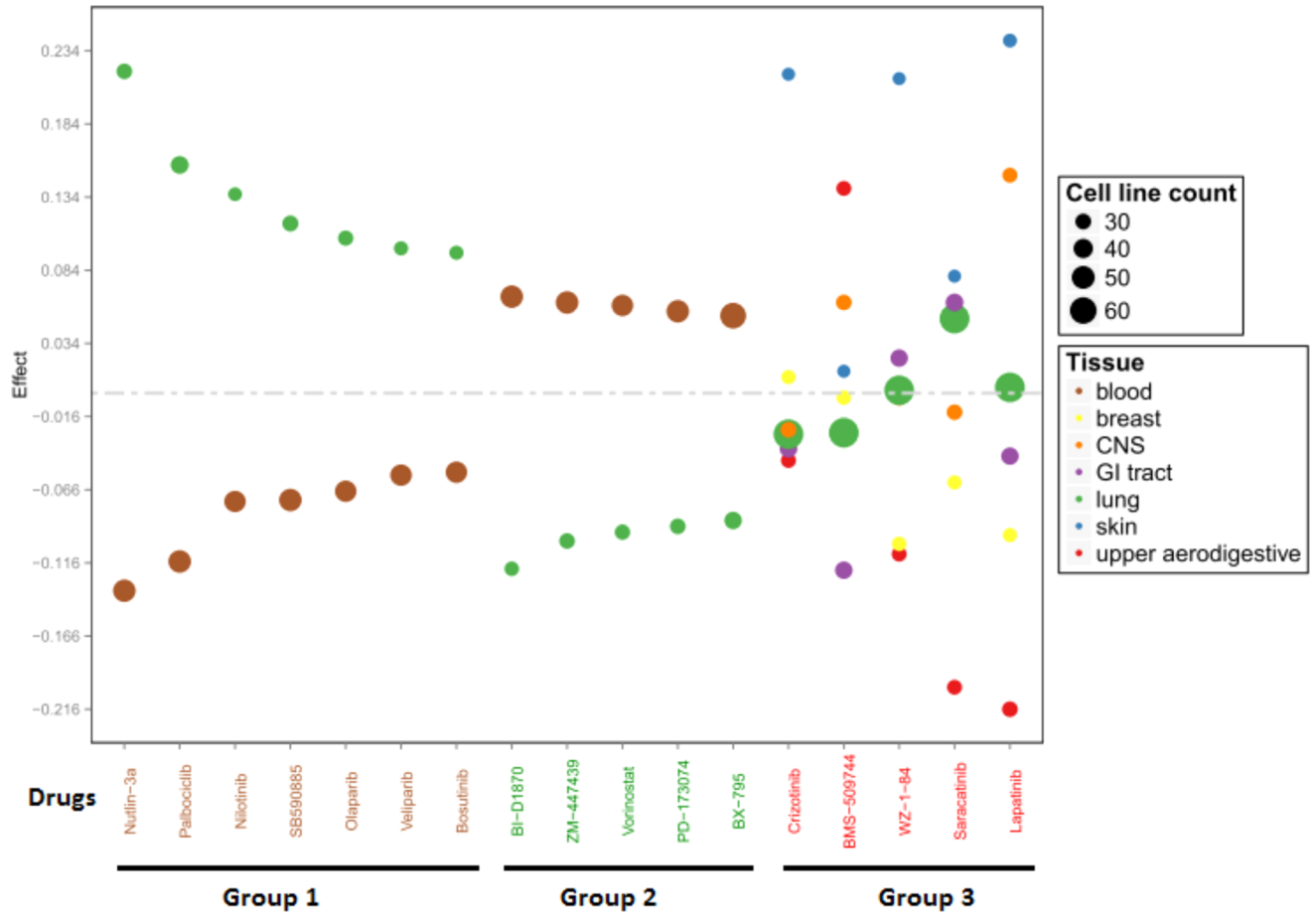

Figure 6. Tissue effects from one-way ANOVA for a set of potentially therapeutic drugs. Each column shows all the tissue effects for one drug. The color represents the cancer tissue type. The size of the circle denotes the number of missing values in the original data for which response values have now been computationally predicted. Effects are calculated as the difference between group mean and grand mean. Smaller values correspond to sensitive tissue types, and larger values correspond to resistant tissue types. Three visually clear and interesting groups of drugs have been denoted by Groups 1, 2, and 3.

Finally, we discuss properties of the full response data, containing both the observed data and the newly predicted values for unobserved drug-cell line combinations (focusing on the seven major tissue types from Figure 6), giving a global view on treatment potential as shown in Figure 7 and Figure S-4 of the Supporting Information). We observe that the drugs camptothecin, doxorubicin, docetaxel, paclitaxel, vinorelbine, vinblastine, epothilone-B, bortezomib, and thapsigargin show efficacy across many cell lines, spanning many cancer tissue types. This is in line with the known evidence about these drugs in NCI database, as many of them have been approved for several types of cancers, and importantly, they are general cytotoxic or antimitotic drugs and therefore affect many, if not all, cancer cell lines (in particular doxorubicin, docetaxel, paclitaxel, vinblastine, and vinorelbine). On the other hand, all cancer types are resistant to the drugs cyclopamine, GDC-0449, LFM-A13, AICAR, metformin, WZ-1-84, NSC-87877, KIN001-135, KU-55933, lenalidomide, ABT-888, DMOG, JNK-Inhibitor-VIII, and BIRB-0796. Some aspects of drug activity become only visible in the map that includes the newly predicted values; they were not evident from the observed data only. One example is the finding that the strongest response of the drug AZ628 is achieved in a large set of skin cancer cell lines. The efficacy of this drug on melanoma, a type of skin cancer, is known from the literature.[39] Another interesting observation from the global map is that dasatinib and WH-4-023 show in large parts similar response patterns and strong efficacy for a small number of blood cell lines, which is consistent with the NCI annotation of dasatinib. The two drugs have some structural similarities on the 2D level and share certain targets (SRC family and ABL). Bosutinib also hits these targets and has similar but weaker response patterns. Mitomycin-C exhibits activity spanning various tissue types and has been approved for GI tract and pancreatic cancers.

The fully predicted drug response map can be used as a resource for generating new hypotheses on cancer drug treatment and repositioning of drugs, suggesting targeted experiments for further studies. For instance, the reddish vertical stripes seen for several drugs suggest wide effective responses and broad applicability, whereas small red patches exhibit more localized responses and applicability for specific types of cancer (e.g., blood).

Novel Task of Personalized QSAR Analysis. Finally, we address the novel task of predicting responses to new drugs for new cell lines. This can be considered as personalized QSAR analysis, i.e., finding suitable drugs for new cancer cell line(s) or patient(s) (Figure 2). When predicting values for combinations of held-out drugs and held-out cell lines, KBMF achieved MSE, R^2, and R_p values of 0.78 ± 0.012 (0.92), 0.20 and 0.52, respectively. Because this prediction task is very challenging, the

dx.doi.org/10.1021/ci500152b | J. Chem. Inf. Model. XXXX, XXX, XXX−XXX

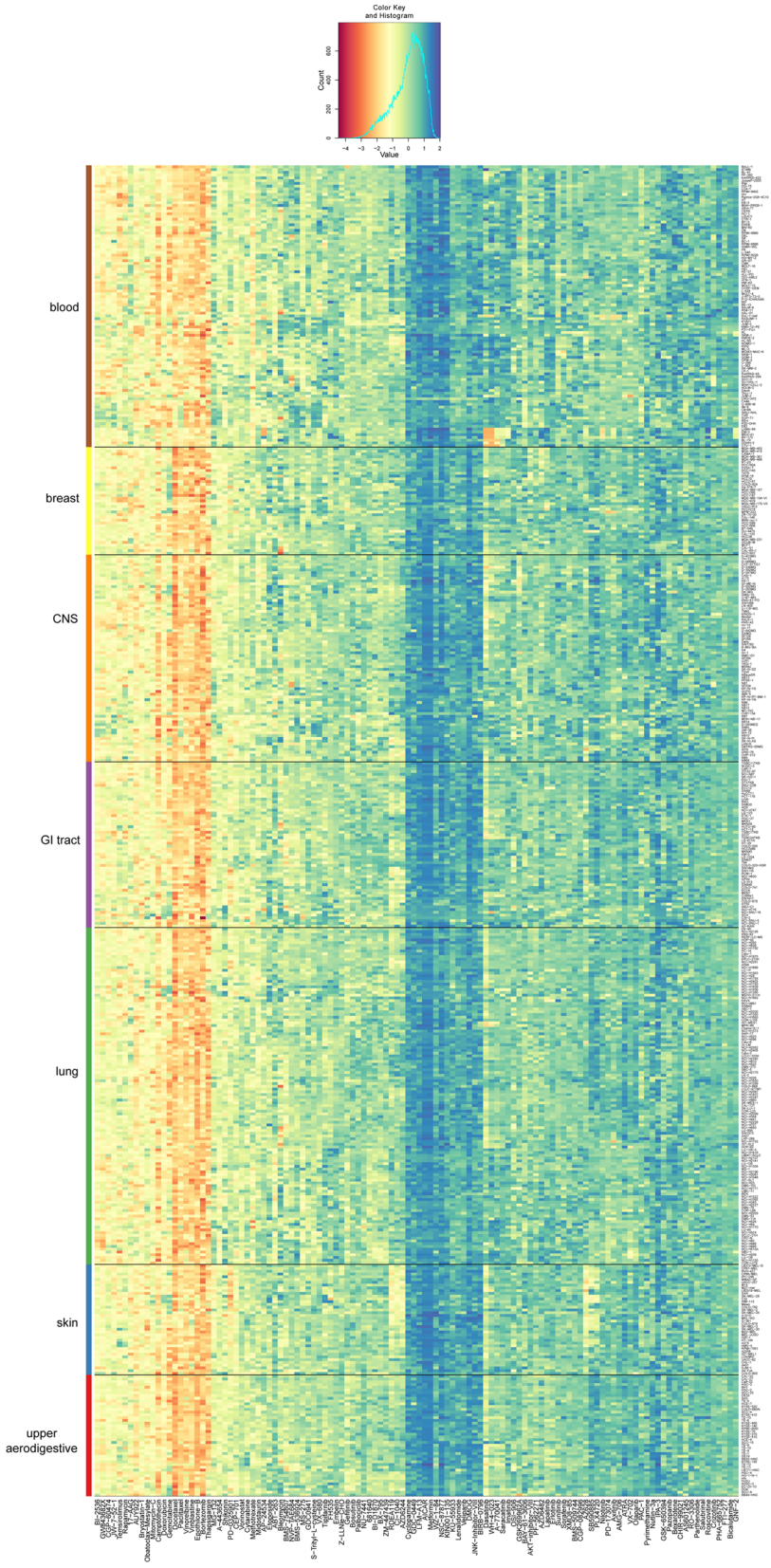

Figure 7. Global drug response map showing responses of 482 cancer cell lines from seven tissue types to 116 drugs. The map was compiled from predicted missing data (25.4%) and observed data. The annotation bar (left) represents the cell line tissue type. The color key (top) shows the range of the log IC_{50} responses.

performance is lower than for the task where the set of cell lines is known beforehand (Table 2). However, when the cell line is new, the approach is significantly better (with a p-value <0.01; Table S-13 and S-14, Supporting Information) than what is

dx.doi.org/10.1021/ci500152b | J. Chem. Inf. Model. XXXX, XXX, XXX−XXX

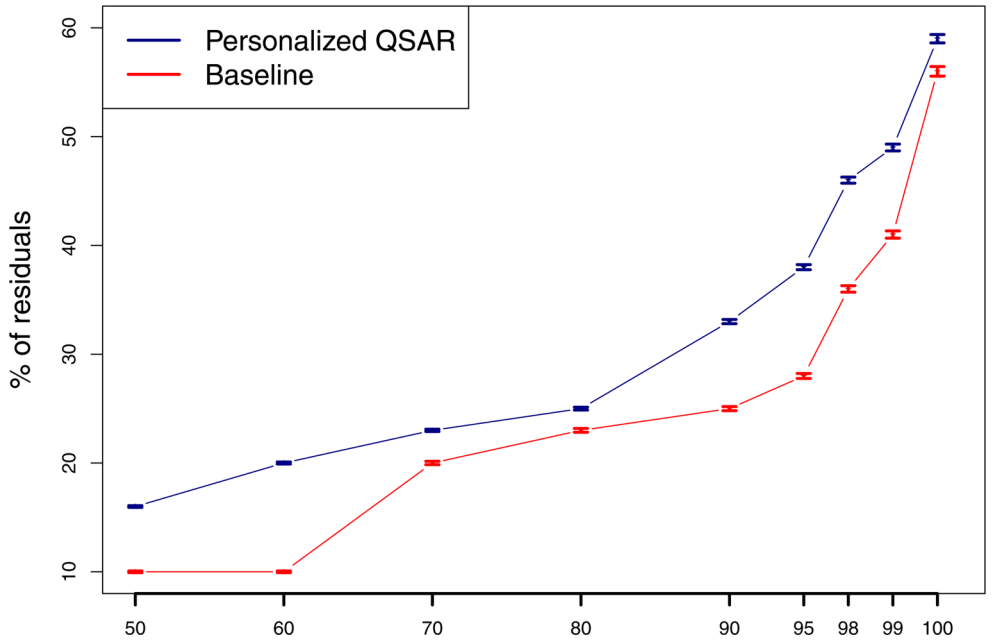

Figure 8. Percentage of prediction residuals (y-axis) falling into percentiles around the mean of missing value prediction residuals (x-axis). The bars around the points denote the standard deviation at a particular percentile. Personalized QSAR (blue color): predicting responses to new drugs and new cell lines using KBMF approach. Baseline (red color): predicting the mean of the training data. The KBMF method outperforms the baseline approach in the challenging task of predicting personalized QSAR responses. Full residual distributions of the baseline, personalized QSAR prediction, and missing value prediction can be found in Figure S-5 of the Supporting Information.

available as baseline. Predicting the mean of the training data yields a MSE of 1.08 ± 0.015 (1.24).

As this is a new task, we cannot compare to existing approaches, and we quantify the quality of personalized QSAR predictions by using the easier prediction tasks above as a yardstick. We chose the missing value predictions (i.e., warm-start) as the reference and checked the fraction of residuals (observed value minus predicted value) falling into percentiles around the mean of the warm-start distribution (Figure 8). About 60% of the personalized QSAR prediction residuals and 55% of the baseline residuals are covered by the whole range of missing value prediction residuals, whereas at the 60% quantile, 20% of personalized QSAR prediction residuals, and 10% of baseline residuals are covered. In summary, while a larger amount of available information increases the prediction accuracy, the proposed KBMF method outperforms the available baseline in the challenging *de novo* prediction task.

To further support our findings, we additionally compared the distribution of entrywise residuals with the residual distributions from other prediction tasks (Figure S-5, Supporting Information). The missing value prediction task where both the cell line and the drug have been observed earlier (but not in combination) has the narrowest residual distribution, peaking at zero. The other prediction tasks yield much more widespread distributions, differing less from each other than from the missing value prediction scenario.

These results show that it is possible to tackle the new personalized QSAR prediction task with machine learning approaches. It would be possible to adapt some of the other recent methods[4] to the task as well, and assessing the relative merits and clinical impact will naturally need further studies.

CONCLUSION

We presented an extended QSAR analysis approach using kernelized Bayesian matrix factorization (KBMF). Our two main conceptual contributions are (i) an integrative QSAR approach predicting responses to new drugs for a panel of known cell lines and (ii) a personalized QSAR approach predicting responses to new drugs for new cell lines. Earlier methods have not been available for the personalized QSAR task, and in the simpler tasks, our experiments have shown that KBMF was at least as good as the existing methods. A case study on the large Sanger cancer drug response data set demonstrated the feasibility of these prediction scenarios and showed that the use of multiple side information sources for both drugs and cell lines simultaneously improved the prediction performance. In particular, combining chemical and structural drug properties, target information, and genomic properties yielded more powerful drug response predictions than drug descriptors or targets alone. Furthermore, KBMF achieved high accuracy in predicting missing drug responses, allowing for construction of a complete drug response map covering 116 drugs and 482 cell lines from seven tissue types. The described method is able to tackle various relevant prediction tasks related to drug response analysis and other kinds of quantitative matrix prediction from side information. It will help in further studies to suggest targeted experiments for potential therapies.

ASSOCIATED CONTENT

Supporting Information

Benchmark experiment on QSAR data sets and their cross-validation results (text, Tables S-1 and S-2); and experimental details, evaluation criteria, and additional results from integrative and personalized QSAR analysis using the Sanger data set (text, Tables S-3 to S-14, Figures S-1 to S-5). This material is available free of charge via the Internet at http://pubs.acs.org.

dx.doi.org/10.1021/ci500152b | J. Chem. Inf. Model. XXXX, XXX, XXX−XXX

AUTHOR INFORMATION

Corresponding Authors

*E-mail: muhammad.ammad-ud-din@aalto.fi (M.A.).
*E-mail: samuel.kaski@aalto.fi (S.K.).

Notes

The authors declare no competing financial interest.

ACKNOWLEDGMENTS

We are grateful to Suleiman A. Khan, Sohan Seth, Juuso Parkkinen, and John-Patrick Mpindi for helpful comments. This work was financially supported by the Academy of Finland (Finnish Center of Excellence in Computational Inference Research COIN, Grant 251170, Grant 140057, and Biocenter Finland/DDCB). We acknowledge the computational resources provided by Aalto Science-IT project and CSC-IT Center for Science Ltd.

REFERENCES

(1) Garnett, M. J.; Edelman, E. J.; Heidorn, S. J.; Greenman, C. D.; Dastur, A.; Lau, K. W.; Greninger, P.; Thompson, I. R.; Luo, X.; Soares, J.; et al. Systematic identification of genomic markers of drug sensitivity in cancer cells. *Nature* **2012**, *483*, 570−575.

(2) Heiser, L. M.; Sadanandam, A.; Kuo, W.-L.; Benz, S. C.; Goldstein, T. C.; Sam, Ng.; Gibb, W. J.; Wang, N. J.; Ziyad, S.; Tong, F.; et al. Subtype and pathway specific responses to anticancer compounds in breast cancer. *Proc. Natl. Acad. Sci. U.S.A.* **2012**, *109*, 2724−2729.

(3) Barretina, J.; Caponigro, G.; Stransky, N.; Venkatesan, K.; Margolin, A. A.; Kim, S.; Wilson, C. J.; Lehar, J.; Kryukov, G. V.; Sonkin, D.; et al. The Cancer Cell Line Encyclopedia enables predictive modelling of anticancer drug sensitivity. *Nature* **2012**, *483*, 603−607.

(4) Menden, M. P.; Iorio, F.; Garnett, M.; McDermott, U.; Benes, C.; Ballester, P. J.; Saez-Rodriguez, J. Machine learning prediction of cancer cell sensitivity to drugs based on genomic and chemical properties. *PLoS One* **2013**, *8*, e61318.

(5) Costello, J. C.; Heiser, L. M.; Georgii, E.; Gönen, M.; Menden, M. P.; Wang, N. J.; Bansal, M.; Ammad-ud-din, M.; Hintsanen, P.; Khan, S. A.; Mpindi, J.-P.; Kallioniemi, O.; NCI Dream Community; Honkela, A.; Aittokallio, T.; Wennerberg, K.; Collins, J. J.; Gallahan, D.; Singer, D.; Saez-Rodriguez, J.; Kaski, S.; Gray, J. W.; Stolovitzky, G. A community effort to assess and improve drug sensitivity prediction algorithms. *Nat. Biotechnol.* **2014**, DOI: 10.1038/nbt.2877.

(6) Perkins, R.; Fang, H.; Tong, W.; Welsh, W. J. Quantitative structure-activity relationship methods: Perspectives on drug discovery and toxicology. *Environ. Toxicol. Chem.* **2003**, *22*, 1666−1679.

(7) Wellcome Trust Sanger Institute, Genomics of Drug Sensitivity in Cancer, 2012. http://www.cancerrxgene.org/ (accessed July 1, 2012).

(8) Myint, K. Z.; Xie, X.-Q. Recent advances in fragment-based QSAR and multi-dimensional QSAR methods. *Int. J. Mol. Sci.* **2010**, *11*, 3846−3866.

(9) Shao, C.-Y.; Chen, S.-Z.; Su, B.-H.; Tseng, Y. J.; Esposito, E. X.; Hopfinger, A. J. Dependence of QSAR models on the selection of trial descriptor sets: A demonstration using nanotoxicity endpoints of decorated nanotubes. *J. Chem. Inf. Model.* **2013**, *53*, 142−158.

(10) Papa, E.; Villa, F.; Gramatica, P. Statistically validated QSARs, based on theoretical descriptors, for modeling aquatic toxicity of organic chemicals in *Pimephales promelas* (Fathead Minnow). *J. Chem. Inf. Model.* **2005**, *45*, 1256−1266.

(11) Kraker, J. J.; Hawkins, D. M.; Basak, S. C.; Natarajan, R.; Mills, D. Quantitative structure-activity relationship (QSAR) modeling of juvenile hormone activity: Comparison of validation procedures. *Chemom. Intell. Lab. Syst.* **2007**, *87*, 33−42.

(12) Luilo, G. B.; Cabaniss, S. E. Quantitative structure-property relationship for predicting chlorine demand by organic molecules. *Environ. Sci. Technol.* **2010**, *44*, 2503−2508.

(13) Matysiak, J. QSAR of antiproliferative activity of N-substituted 2-amino-5-(2,4-dihydroxyphenyl)-1,3,4-thiadiazoles in various human cancer cells. *QSAR Comb. Sci.* **2008**, *27*, 607−617.

(14) Rogers, D.; Hopfinger, A. J. Application of genetic function approximation to quantitative structure−activity relationships and quantitative structure−property relationships. *J. Chem. Inf. Comput. Sci.* **1994**, *34*, 854−866.

(15) Zheng, W.; Tropsha, A. Novel variable selection quantitative structure-property relationship approach based on the k-nearest-neighbor principle. *J. Chem. Inf. Comput. Sci.* **2000**, *40*, 185−194.

(16) Kompany-Zareh, M.; Omidikia, N. Jackknife-based selection of Gram Schmidt orthogonalized descriptors in QSAR. *J. Chem. Inf. Model.* **2010**, *50*, 2055−2066.

(17) Cramer, R. D.; Patterson, D. E.; Bunce, J. D. Comparative molecular field analysis (CoMFA). 1. Effect of shape on binding of steroids to carrier proteins. *J. Am. Chem. Soc.* **1988**, *110*, 5959−5967.

(18) Hasegawa, K.; Funatsu, K. Evolution of PLS for Modeling SAR and omics Data. *Mol. Inf.* **2012**, *31*, 766−775.

(19) Musumarra, G.; Condorelli, D. F.; Costa, A. S.; Fichera, M. A multivariate insight into the in-vitro antitumour screen database of the National Cancer Institute: Classification of compounds, similarities among cell lines and the influence of molecular targets. *J. Comput.-Aided Mol. Des.* **2001**, *15*, 219−234.

(20) Yamanishi, Y.; Pauwels, E.; Kotera, M. Drug side-effect prediction based on the integration of chemical and biological spaces. *J. Chem. Inf. Model.* **2012**, *52*, 3284−3292.

(21) Liu, P.; Long, W. Current mathematical methods used in QSAR/QSPR studies. *Int. J. Mol. Sci.* **2009**, *10*, 1978−1998.

(22) Sutherland, J. J.; O'Brien, L. A.; Weaver, D. F. A comparison of methods for modeling quantitative structure-activity relationships. *J. Med. Chem.* **2004**, *47*, 5541−5554.

(23) Lusci, A.; Pollastri, G.; Baldi, P. Deep architectures and deep learning in chemoinformatics: the prediction of aqueous solubility for drug-like molecules. *J. Chem. Inf. Model.* **2013**, *53*, 1563−1575.

(24) Mullen, L. M.; Duchowicz, P. R.; Castro, E. A. QSAR treatment on a new class of triphenylmethyl-containing compounds as potent anticancer agents. *Chemom. Intell. Lab. Syst.* **2011**, *107*, 269−275.

(25) Lee, A. C.; Shedden, K.; Rosania, G. R.; Crippen, G. M. Data mining the NCI60 to predict generalized cytotoxicity. *J. Chem. Inf. Model.* **2008**, *48*, 1379−1388.

(26) Gao, J.; Che, D.; Zheng, V.; Zhu, R.; Liu, Q. Integrated QSAR study for inhibitors of hedgehog signal pathway against multiple cell lines: A collaborative filtering method. *BMC Bioinf.* **2012**, *13*, 186.

(27) Gönen, M. Predicting drug-target interactions from chemical and genomic kernels using Bayesian matrix factorization. *Bioinformatics* **2012**, *28*, 2304−2310.

(28) Gönen, M.; Khan, S.; Kaski, S. Kernelized Bayesian Matrix Factorization. In *Proceedings of the 30th International Conference on Machine Learning (ICML)*, Atlanta, GA, U.S.A., June 16−20, 2013, pp 864−872.

(29) Schölkopf, B.; Smola, A. J. *Learning with Kernels: Support Vector Machines, Regularization, Optimization, and Beyond*; MIT Press: Cambridge, MA, 2002; Chapter 15, pp 457−468.

(30) Beal, M. J. Variational Algorithms for Approximate Bayesian Inference. Ph.D. Thesis, Gatsby Computational Neuroscience Unit, University College, London, 2003.

(31) Bolton, E. E.; Wang, Y.; Thiessen, P. A.; Bryant, S. H. PubChem: Integrated platform of small molecules and biological activities. *Annu. Rep. Comput. Chem.* **2008**, *4*, 217−241.

(32) Yap, C. W. PaDEL-descriptor: An open source software to calculate molecular descriptors and fingerprints. *J. Comput. Chem.* **2011**, *32*, 1466−1474.

(33) National University of Singapore, PaDEL-descriptor: An Open Source Software to Calculate Molecular Descriptors and Fingerprints, 2011. http://padel.nus.edu.sg/software/padeldescriptor/ (accessed January 15, 2013).

(34) Cruciani, G.; Crivori, P.; Carrupt, P.-A.; Testa, B. Molecular fields in quantitative structure−permeation relationships: The VolSurf approach. *J. Mol. Struct.* **2000**, *503*, 17−30.

(35) Pastor, M.; Cruciani, G.; McLay, I.; Pickett, S.; Clementi, S. GRid-INdependent descriptors (GRIND): A novel class of alignment-independent three-dimensional molecular descriptors. *J. Med. Chem.* **2000**, *43*, 3233−3243.
(36) Duran, A.; Martinez, G. C.; Pastor, M. Development and validation of AMANDA, a new algorithm for selecting highly relevant regions in molecular interaction fields. *J. Chem. Inf. Model.* **2008**, *48*, 1813−1823.
(37) Durán, A.; Zamora, I.; Pastor, M. Suitability of GRIND-based principal properties for the description of molecular similarity and ligand-based virtual screening. *J. Chem. Inf. Model.* **2009**, *49*, 2129−2138.
(38) National Institutes of Health, National Cancer Institute (NCI), 1971. http://www.cancer.gov/ (accessed May 10, 2013).
(39) Hatzivassiliou, G.; et al. RAF inhibitors prime wild-type RAF to activate the MAPK pathway and enhance growth. *Nature* **2010**, *464*, 431−435.